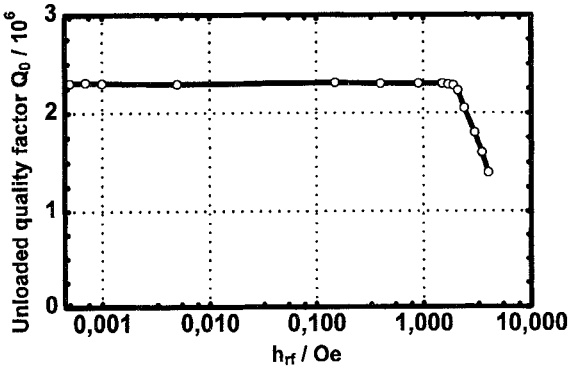

Fig. 4. Dependence of unloaded quality factor (Q_o) for a dielectric sapphire resonator using 2 in TBCCO-films on the surface magnetic field (h_{rf}) at 5.6 GHz and 77 K.

the Tl-2223 phase with two Tl-O planes. At present the rf-power dependence of R_s is in detail not clear.

V. Conclusion

The two step technology allows to prepare high quality 2-in Tl-2223 superconducting films with surface resistance values (R_s) smaller than 100 $\mu\Omega$ at 5.6 GHz and 77 K. The use of these films in sapphire dielectric resonators yields resonators for the C-band with very high unloaded quality factors ($Q_o > 2 \times 10^6$ at 77 K). Such high quality factors are only reached with Whispering Gallery Modes sapphire resonators and Fabry-Perot mirror resonators, but these resonators are very voluminous and heavy below 10 GHz. Acoustic resonators such as SAW (surface acoustic wave), BAW (bulk acoustic wave) and HBAR (high overtone bulk acoustic resonators) are limited to operating frequencies below 1 GHz and therefore require frequency multiplication for application in the C-band and X-band with the consequence of a large increase in noise. The unloaded quality factor of normal-conducting dielectric resonators with ceramic or sapphire pucks is two orders of magnitude lower than the Q_o-values of the described superconducting resonators. Therefore, superconducting dielectric sapphire resonators on compact stirling cycle cryocoolers can be used in microwave oscillators with very low phase noise behavior. A typical industrial application for these oscillators is in cryoradar systems with an improved detection threshold.

References

[1] W. E. Courtney, "Analysis and evaluation of a method of measuring the complex permittivity and permeability of microwave insulators," *IEEE Trans. Microwave Theory Tech.*, vol. 18 no. 3, pp. 476–485, 1970.

[2] J. Krupka, M. Klinger, M. Kuhn, A. Baranyak, M. Stiller, J. Hinken, and J. Modelski, "Surface resistance measurements of films by means of sapphire dielectric resonators," *IEEE Trans. Appl. Superconduct.*, vol. 3 no. 1, pp. 3043–3048, 1993.

[3] C. Wilker, Z-Y Shen, V. X. Nguyen, and M. S. Brenner, "A sapphire resonator for microwave characterization of superconducting thin films," *IEEE Trans. Appl. Superconduct.*, vol. 3 no. 1, pp. 1457–1460, 1993.

[4] Z. Y. Shen, C. Wilker, P. Pang, W. L. Holstein, D. Face, and D. J. Kountz, "High Tc superconductor-sapphire microwave resonator with extremely high Q-values up to 90 K," *IEEE Trans. Microwave Theory Tech.*, vol. 40 no. 12, pp. 2424–2432, 1992.

[5] M. Manzel, H. Bruchlos, E. Steinbeiß, T. Eick, M. Klinger, J. Fuchs, and B. Kley, "TlBaCaCuO-films for passive microwave devices," *Physica C*, no. 201, pp. 337–339, 1992.

[6] M. Manzel, H. Bruchlos, F. Sandiumenge, G. Bruchlos, M. Kuhn, M. Klinger, and J. H. Hinken, "Planar and cavity microwave resonators using TBCCO-films," in *Applied Superconductivity*, H.C. Freyhardt, Ed. Oberursel, Germany: DGM Informationsgesellschaft Verlag, 1993, vol. 2, pp. 995–998.

[7] J. Krupka, private communication.

[8] S. Huber, M. Manzel, H. Bruchlos, S. Hensen, and G. Müller, "Thallium-based high-Tc films with very low surface impedance," *Physica C*, no. 244, pp. 337–340, 1995.

[9] W. L. Holstein, L.A. Parisi, C. Wilker and R.B. Flippen, "Epitaxial $Tl_2Ba_2Ca_2Cu_3O_{10}$ films with very low microwave surface resistance up to 110 K," *IEEE Trans. Appl. Superconduct.*, vol. 3 no. 1, pp. 1197–1200, 1993.

[10] W. L. Holstein and L. A. Parisi, "Highly oriented very low surface resistance $Tl_2Ba_2CaCu_2O_8$ Films on $NdGaO_3$ and $LaAlO_3$," *Appl. Phys. Lett.*, vol. 60 no. 16, pp. 2014–2019, 1992.

[11] S. Hensen, S. Orbach-Werbig, G. Müller, H. Piel, N. G. Chew, J. A. Edwards, and R. G. Humphreys, "Effect of small changes in metal stoichiometry on microwave losses of epitaxially grown $YBa_2Cu_3O_{7-\delta}$ films," *Applied Superconductivity*, H.C. Freyhardt, Ed. Oberursel, Germany: DGM Informationsgesellschaft Verlag, 1993, vol. 2, pp. 1053–1056.

[12] M. Manzel, H. Bruchlos, S. Huber, M. Kuhn, J. Keppler, and J. H. Hinken, "Preparation and microwave characterization of TBCCO-films," *Physica C*, no. 235–240, pp. 713–714 1994.

Twenty-GHz Broadband Microstrip Array with Electromagnetically Coupled High T_c Superconducting Feed Network

Jeffrey S. Herd, Livio D. Poles, James P. Kenney, John S. Derov, Michelle H. Champion, Jose H. Silva, Marat Davidovitz, Kenneth G. Herd, William J. Bocchi, Steven D. Mittleman, and Dallas T. Hayes

***Abstract*— The use of high-temperature superconducting (HTS) feed lines and phase shifters can substantially improve the performance of microwave and millimeter-wave printed phased array antennas. A novel antenna architecture is described that provides a broadband radiating aperture to be used as a scanning array with compatible low-loss HTS phase shifters. The approach follows an earlier design demonstrated at 12 GHz, and this work extends the approach to 20 GHz. The antenna design, radiation patterns, bandwidth measurements, and thermal analysis are reported. A prototype thermal isolator design is described that reduces the heat load of coaxial interconnections between cryocooled and room temperature systems.**

I. Introduction

Ohmic losses in passive microwave and millimeter-wave printed phased array antennas severely limit the achievable gain and noise figure. Active antenna arrays utilize amplifiers at each element to compensate for losses, but practical factors such as heat dissipation, stability, calibration, and reliability introduce significant technological challenges. Alternatively, components fabricated using high-

Manuscript received October 23, 1995; revised February 22, 1996.

J. S. Herd, L. D. Poles, J. P. Kenney, J. S. Derov, M. H. Champion, J. H. Silva, M. Davidovitz, W. J. Bocchi, S. D. Mittleman, and D. T. Hayes are with Rome Laboratory, Hanscom AFB, MA 01731-3010 USA.

K. G. Herd is with General Electric Corporate Research and Development, Schenectady, NY USA.

Publisher Item Identifier S 0018-9480(96)04786-2.

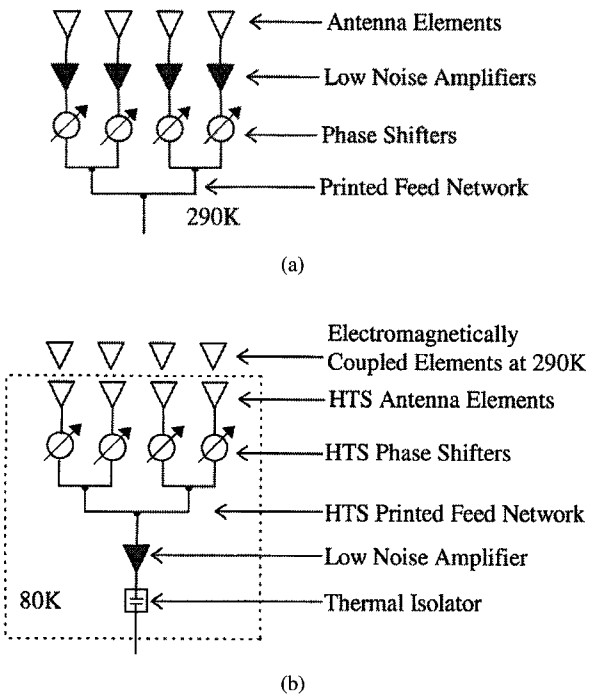

Fig. 1. (a) Active phased array architecture. (b) Electromagnetically coupled high temperature superconducting array architecture.

temperature superconducting (HTS) thin films can be incorporated into array architectures to dramatically improve performance [1]–[4].

Two significant sources of loss in printed phased arrays are the corporate feeding network and the phase shifters. Typical MESFET switched-line phase shifters have 2–3 dB of insertion loss per bit [6], [7]. A variety of different HTS phase shifter architectures have been developed that dramatically reduce the insertion loss. They include a thermally switched delay line phase shifter with approximately 0.5 dB/bit insertion loss at 20 GHz [8] and a distributed Josephson inductance phase shifter with less than 1 dB of insertion loss for 250° of continuous phase shift at 60 GHz [9]. The latter device requires approximately 1 dB of amplitude control at each phase shifter to compensate for insertion loss variations as a function of the control field. Recently, a planar HTS ferrite phase shifter has been demonstrated with over 700° of continuous phase shift and 0.7 dB of insertion loss at 10 GHz [10], [11].

Fig. 1 shows two candidate architectures for microwave and millimeter-wave printed phased array antennas. The first is an active array on GaAs operating at 290°K with a low-noise amplifiers and phase shifters behind each element. The second is a passive array on $LaAlO_3$ with HTS phase shifters and feed network followed by a low-noise amplifier operating at 80°K inside a cryocooled vacuum enclosure. The cryocooled network is electromagnetically coupled to parasitic antenna elements outside at 290°K and has a thermally isolated coaxial cable at the output.

A performance comparison can be made of the two array architectures. The antenna system figure of merit is defined as the antenna gain G divided by the system noise temperature T referred to the array aperture. The gain to noise temperature ratio (G/T) for a planar 1024-element active microstrip array at 20 GHz on GaAs ($\varepsilon_r = 12.8$, $\tan\delta = 6 \times 10^{-3}$) at 290°K with a directive gain of 35.0 dB, antenna noise temperature of 60°K, a low noise amplifier at each element with a noise figure of 2.0 and gain of 22.0 dB [12], 8.0 dB of loss in a 4-bit phase shifter at each element [6], and 9.3 dB of loss in the feed network ($\alpha = 0.4$ dB/cm) is calculated to be $G/T = 9.9$ dB. The feed network loss is determined for a square array with N elements as $P_L^{feed} = (N^{1/2} - 1)(\alpha d)$ in dB [5], where d is the element spacing and α is the loss per centimeter on a microstrip transmission line. The loss in the power dividers is assumed to be primarily mismatch loss and is approximately the same for both the normal metal and HTS versions. It is therefore left out of the loss comparison. The same size superconducting array at 20 GHz on $LaAlO_3$ ($\varepsilon_r = 23.7$, $\tan\delta = 5 \times 10^{-4}$) with HTS phase shifter loss of 0.7 dB [10], feed network loss of 0.4 dB, ($\alpha = 0.018$ dB/cm), followed by a low-noise amplifier with a noise figure of 0.5 at 80°K has a $G/T = 15.2$ dB, which is a 5.3-dB improvement. This example clearly demonstrates superior performance for a cooled passive HTS antenna array versus an active normal metal array at room temperature. It should be noted that the active array would also have a G/T of 15.2 dB at an operating temperature of 80°K, assuming a cooled LNA noise figure of 0.5 dB.

The implementation of HTS components in phased-array systems presents a unique set of challenges. To begin with, the system must be cooled to cryogenic temperatures, and any connections with uncooled components must be carefully designed to minimize RF insertion loss and thermal heat transfer. Furthermore, a radiating aperture must be designed that can operate over the desired scan volume and bandwidth with minimal pattern degradation by the cooling apparatus. Additional constraints are imposed by the high dielectric constant of $LaAlO_3$ substrates, which are most commonly used in RF applications [13]. It has been reported that the dielectric constant of $LaAlO_3$ varies spatially by approximately 2% across a given sample due to twinning defects [14]. This variation could cause shifts in the antenna impedance across the array. The high dielectric constant also makes it difficult to obtain bandwidths of over 1% for 2 : 1 VSWR using conventional single-layer microstrip elements [15]. Mutual coupling between elements of a scanning array causes impedance mismatch as a function of scan angle, further reducing the operating bandwidth over a specified scan volume [16]. Surface wave coupling in an electrically thick substrate layer can also produce scan blindness angles in large arrays of printed antennas [17].

This paper describes the development of a 20-GHz microstrip antenna array in which special efforts have been made to overcome or alleviate the difficulties described above and to provide a reliable and well-characterized radiating aperture to be used with appropriate phase shifters when they become available. This work follows an approach demonstrated earlier at 12 GHz [3].

II. Electromagnetically Coupled Array Geometry

The antenna is a multilayer microstrip patch array. As shown in Fig. 2, the structure consists of two dielectric layers separated by a vacuum layer. The lower layer is a 0.254-mm-thick $LaAlO_3$ substrate, upon which an HTS microstrip power combining network and antenna array are fabricated using a laser-ablated 4000-Å c-axis epitaxial YBCO thin film on the upper surface, with a copper ground plane on the lower surface. The superstrate is a 1-mm-thick quartz layer, which serves as a radome that can withstand the atmosphere of pressure difference created by the vacuum inside the cryocooler. An array of electromagnetically coupled copper patch antennas is fabricated on the inner side of the quartz window to enhance the bandwidth of the lower HTS antenna array via double tuning [18]. A 0.5-mm vacuum layer between the warm quartz radome and the cooled $LaAlO_3$ substrate provides thermal isolation. Several low thermal conductivity teflon spacers, each with cross-sectional area of 1 mm^2, are used to maintain precise spacing between the layers. This novel HTS antenna array geometry provides a broader bandwidth and achieves a conformal profile by incorporating the cryocooler window into the design of the antenna.

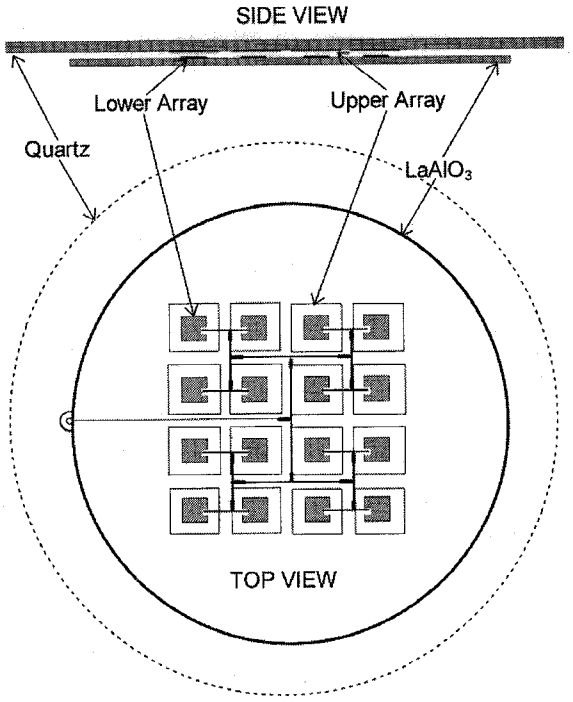

Fig. 2. Multilayer antenna array configuration.

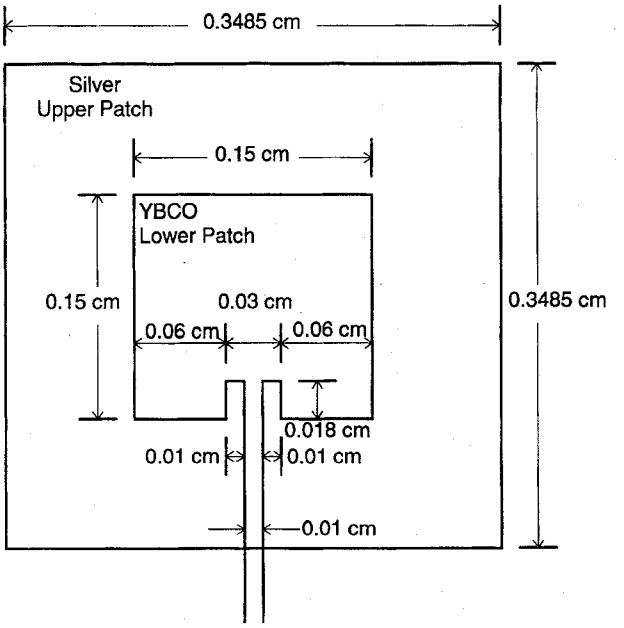

Fig. 3. Stacked microstrip patch dimensions.

III. Analysis and Design

An infinite array spectral dyadic Green's function was chosen to model the antennas, because it includes effects caused by mutual coupling and surface waves [17]. These effects are likely to be significant in a large scanning array printed on a high-permittivity substrate. The method of moments was used to solve the resultant integral equation for the current distribution and input impedance. Sinusoidal entire domain basis functions were used on the patches for the current expansion and test modes. These modes replicate the natural cavity-like behavior of the microstrip antennas and are numerically efficient. The inset microstrip feedline excitation of the lower microstrip antennas was modeled by a vertical electric current ribbon source at the inset point. This approach works particularly well for electromagnetically coupled microstrip antennas, which can typically be matched to a 50-Ω feedline at a small inset from the patch edge [19]. The characteristic impedance and propagation constants of the microstrip lines used in the feed network were obtained by extending techniques developed in [20] to include multiple dielectric layers.

There are several assumptions made in the analysis described above. To begin with, the design assumes that the superconducting materials are infinitesimally thin and that there is no field penetration. In actuality, there will be a slightly slower propagation velocity on the superconducting lines due to finite field penetration. However, the approximation works well for analyzing the impedance and radiation properties of the lines and patches, and the temperature and current densities are well below the critical values. For accurate ohmic loss predictions, a model that includes surface impedance effects must be used [21]–[24]. A second approximation is the neglect of edge effects in the finite array of elements. Elements located on an outer edge of the array will have a slightly different impedance than those at the center because of asymmetric coupling, and this effect is not included in the infinite array model used to design the array.

A 16-element electromagnetically coupled patch array was designed to operate at 20 GHz with maximum bandwidth over a scan cone of $\pm 45^\circ$. The effect of surface wave blindness is minimized by choosing an element spacing of 0.4 λ_0 [19]. As can be seen in Fig. 2, elements in the E-plane of the array are fed on opposite sides. This approach avoids the additional path lengths and radiation from bends in a typical feed network, which feeds all elements on the same side. A phase shift of 180° is built into the feed network to compensate for the anti-phase currents on the alternating elements. Two-stage binomial transformers are used in the T-junction power dividers for maximally flat frequency response over a broad bandwidth. Fig. 3 shows the dimensions of the stacked microstrip patches with the substrates and spacing given in Section II. This geometry was used in the experimental measurements described in Section IV.

IV. Experimental Results

A set of experimental measurements were made to characterize the array and each of the individual components in the system. Fig. 4 shows the different types of test fixtures which were used. Furthest to the left is a two port fixture used to verify the effective dielectric constant and characteristic impedance of various normal metal and HTS microstrip 50-Ω lines printed on $LaAlO_3$ substrates. Second from the left is a three-port fixture used to characterize the performance of the T-junction power dividers with binomial transformers. Second from the right is a single microstrip antenna element fed by a microstrip line. The transparent disc behind it is a 1-mm-thick quartz window with a single electromagnetically coupled patch. On the right is the complete 16-element HTS array and power divider network. Behind is a quartz disc upon which 16 copper patches have been deposited.

Several sets of 50-Ω lines were fabricated to compare the properties of the normal metal lines and cooled HTS lines. It is particularly difficult to make well-calibrated millimeter-wave measurements at cryogenic temperatures, and therefore, the effective dielectric constant was found by measuring the relative insertion phase of several different lengths of printed microstrip line. The outputs of the line were ultrasonically wire bonded to 2.4-mm bulkhead connectors with center pins positioned close to the edge of the $LaAlO_3$ substrate. For the HTS lines, a silver ohmic contact for the wire bonding was patterned on top of the YBCO strip near the edge. Two sets of long and short line lengths were fabricated and tested in both silver and

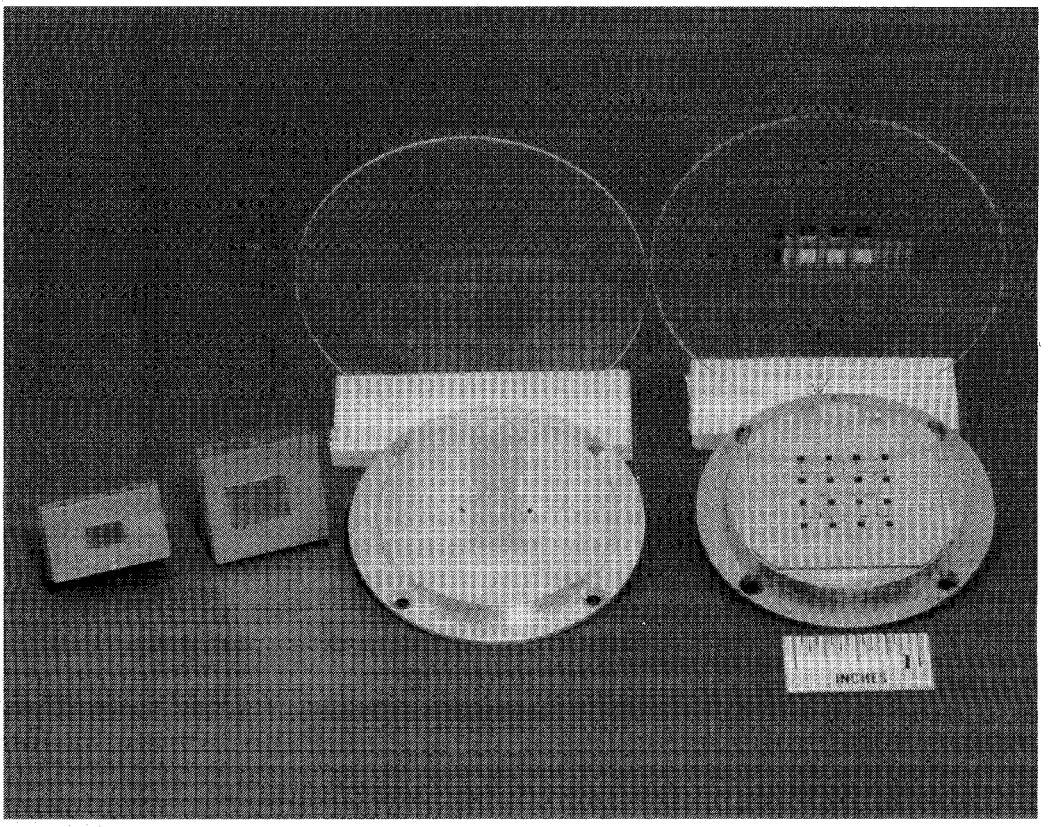

Fig. 4. Test fixtures for array components.

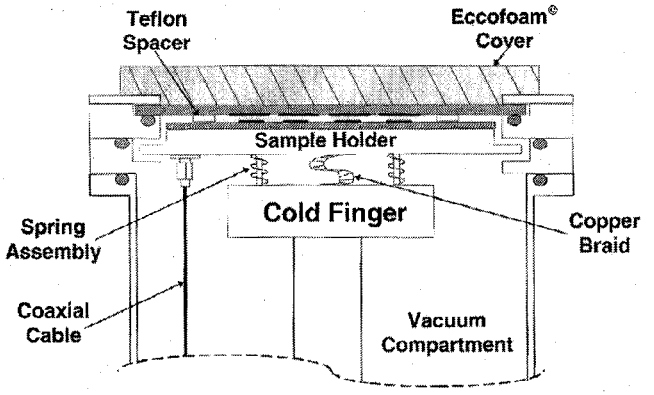

Fig. 5. Array antenna cryocooler mounting.

YBCO at 80°K. The measured return loss of all ports was below −16.7 dB. The worst case phase error was 2° for a designed phase difference of 60°. These results indicate that the measured microstrip line properties are in agreement with the designed values to within the measurement accuracy. The passive circuit properties of HTS circuits such as these can therefore be validated with normal metal prior to final test with HTS materials. This is to be expected, as the kinetic inductance of a 50-Ω microstrip line on a 0.254-mm-thick $LaAlO_3$ substrate is well below 10 nH at low power and at 80°K, whereas the geometrical inductance is approximately 600 nH. It should be noted that some passive HTS circuits such as long delay lines on thin substrates, densely packed structures, operation near T_c or at high power may require modeling of the kinetic inductance effect, which becomes pronounced in these cases [24].

A three-port fixture was used to measure the equal power dividers used in the feed network. This device was only tested in copper at 290°K. The input reflection coefficient was measured to be −15.8 dB, and the difference in transmitted powers in the −3 dB output ports was 0.12 dB.

Measurements were also made of a single electromagnetically coupled copper element at 290°K and a complete array with both copper and HTS feed networks. As shown in Fig. 5, the cooled antenna assemblies are mounted to the cold head of a two-stage closed-cycle helium gas refrigerator. When the system is cooled, the cold finger shrinks by about 0.8 mm, and it is therefore necessary to use a specially devised spring assembly to compensate for the shrinkage, thereby maintaining a constant force against the quartz window by means of the teflon spacers. A good thermal transfer between the movable spring assembly and the cold finger is achieved by connecting them with a flexible copper wire braid. A silicon diode sensor is attached to the sample holder to monitor the temperature during measurements. A machined Eccofoam® plug is flush mounted to the outer surface of the quartz window to prevent frosting.

Antenna radiation patterns and gain measurements were performed with a fully automated Flam and Russell FR959 antenna measurement system and a Hewlett-Packard 8530A receiver. The antenna assembly, vacuum pump, and closed cycle refrigerator were mounted directly onto a rotating antenna positioner for pattern measurements. Antenna gain measurements were made relative to a standard gain horn antenna.

The far field radiation patterns of the antenna arrays were measured over a wide band of frequencies. Fig. 6(a) and (b) shows the patterns of the HTS and copper versions at 19.8 GHz for the E and H plane cuts, respectively. The 3-dB beamwidths are approximately 30°, consistent with the predicted beamwidth of a 4 × 4 element array with 0.4-λ_0 element spacing. The height and location of the sidelobes are as expected. Measurements of gain versus frequency are shown in Fig. 7 for the HTS array at 80°K, the copper array at

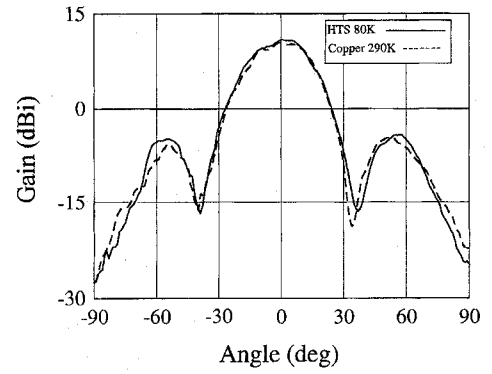

(a)

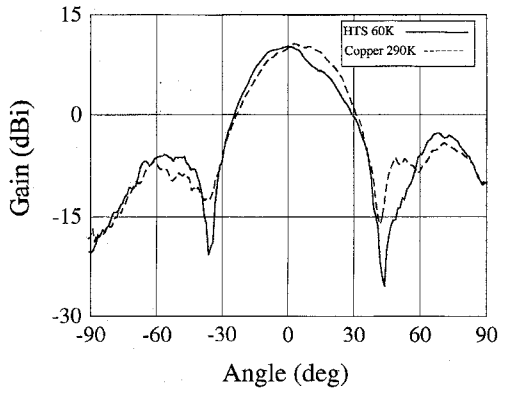

(b)

Fig. 6. (a) E-Plane antenna pattern measurements for HTS and copper arrays. (b) H-plane antenna pattern measurements for HTS and copper arrays.

290°K. The measured maximum gain of 13 dBi is consistent with the predicted area gain for this array of 15 dBi minus approximately 1 dB due to surface wave loss in the substrate [15] and 1 dB due to loss in the connector. The 3-dB radiated power bandwidth is approximately 10% for the HTS and the copper arrays.

The experimental array size is not large enough to show an improvement over the copper version. However, the experiment demonstrates that such an architecture is operational, and future work will seek to quantify the improvement for a larger HTS array with phase shifters versus a normal metal array.

V. Thermal Considerations

The thermal loading of a 4-cm-diameter quartz window at 290°K was analyzed using a two-dimensional (2-D) axisymmetrical finite-element model. Fig. 8 shows the configuration that was used in the calculation. The geometry is not strictly axisymmetric because of the discrete locations of four teflon spacers. However, a good approximation is made by modeling the spacers as a ring with an equivalent surface area. A thermal load of 1.8 W is predicted for an *in-situ* antenna array on the cold head operating at 80°K. The analysis shows that the temperature variation across the sample is small and that the most significant heat loss is via the teflon spacers, which contact both the cooled and warm layers of the structure. A future design will incorporate spacers with minimal surface area and thermal conductivity to reduce the heat loss.

The heat transfer due to the window L_W was measured experimentally by means of a calorimetry technique. In this approach, the response of the cryocooler without the window is measured by recording the steady state temperatures (T_s) of the cryocooler over

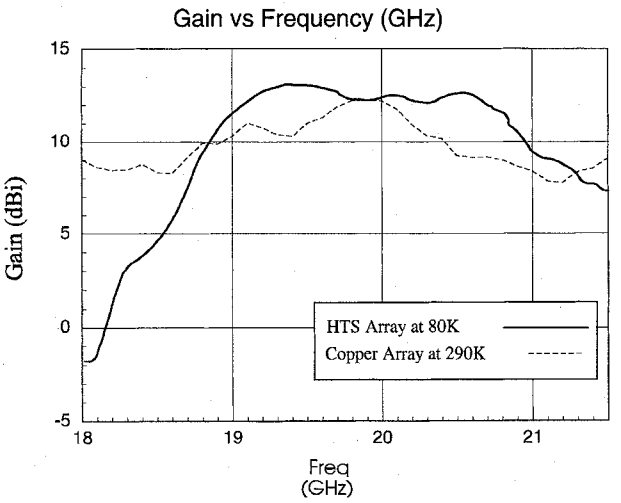

Fig. 7. Measured gain versus frequency for HTS and copper array.

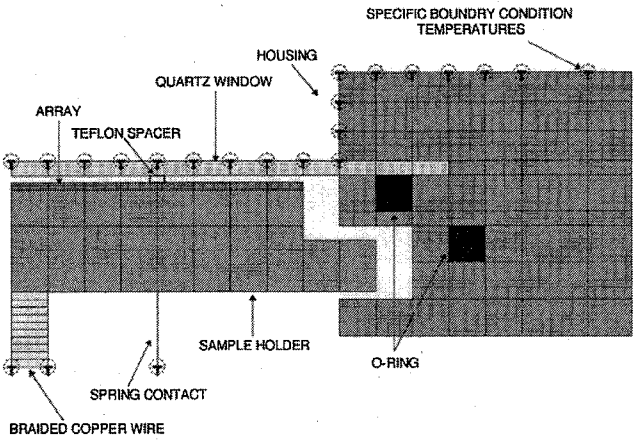

Fig. 8. Geometry for finite-element thermal analysis.

a range of accurately controlled heat loads (L). The temperature T_s of the cryocooler with the window is then measured and L_W is determined from the measured T_s versus L curve. The measured L_W of 2.0 W is in good agreement with the predicted value of 1.8 W.

A second source of heat loss is the interface that is necessary to transfer RF signals between the cooled and warm environments. A small cross-sectional area affords higher thermal resistance and lower heat load, but introduces unacceptable ohmic losses in the system. On the other hand, low ohmic losses require a large cross-sectional area coaxial line, which in turn presents a large thermal loss.

To alleviate this problem, a low RF insertion loss thermal isolator has recently been designed [25]. A similar concept has been reported earlier [26]. The device, shown in Fig. 9, employs a circumferential gap in a rectangular waveguide. The microwave transmission properties of the waveguide are minimally disturbed by the gap, and the radiative and convective heat exchange across the gap is negligible. The alignment of the waveguides on either side of the gap is maintained by a high strength foam that encases the waveguide. A measurement of a prototype isolator utilizing K_a-band (WR-42) rectangular waveguide has less than 0.5-dB insertion loss over a wide frequency band and heat load of 0.4 W with temperatures of 290°K and 80°K at the two inputs. Commercially available 0.141-in-diameter cryogenic coaxial cable has similar heat transfer properties, but introduces a loss that increases linearly with cable length, (e.g., 0.6 dB/ft). The isolator can be connected in series with low RF

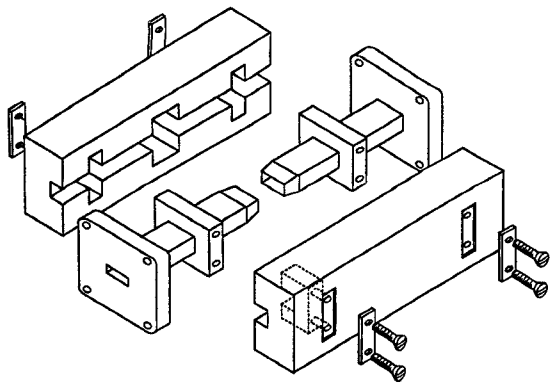

Fig. 9. Exploded view of thermal isolator.

insertion loss coaxial cables or waveguide on either side, since the thermal path resistance is established primarily in the isolator.

The prototype isolator design has not been fully optimized for minimum heat transfer and RF insertion loss. There is a trade-off between the mechanical stability provided by the encasing foam and the heat loss due to conductive heat transfer through the foam. A future design will optimize the thermal and mechanical properties of the encasing foam and is expected to further reduce the heat transfer through the isolator by at least a factor of 10.

VI. Conclusion

A novel HTS antenna array architecture has been developed for use at 20 GHz. The electromagnetically coupled microstrip antenna design provides a broader bandwidth than for conventional microstrip elements, and removes the need for a radome. The microstrip transmission lines, power dividers, and antenna elements have been individually characterized prior to integration of a 16-element array. Measured radiation patterns and gain show excellent agreement with predicted performance.

A thermal analysis has been made of the structure, and the measured heat load agrees closely with the predicted value. A thermal isolator has been developed to reduce the heat transfer via the coaxial connections between the cooled and warm external environments.

In the future, low-loss HTS phase shifters will be incorporated to provide wide-angle electronic scanning capability.

References

[1] R. C. Hansen, "Superconducting antennas," *IEEE Trans. Aerosp. Electron. Syst.*, vol. 26, no. 2, pp. 345–354, Mar. 1990.

[2] J. T. Williams and S. A. Long, "High temperature superconductors and their application in passive antenna systems," *IEEE Antennas Propagat. Mag.*, vol. 32, no. 4, Aug. 1990.

[3] J. S. Herd, D. T. Hayes, J. P. Kenney, L. D. Poles, K. G. Herd, and W. G. Lyons, "Experimental results on a scanned beam microstrip antenna array with a proximity coupled YBCO feed network," *IEEE Trans. Appl. Supercond.*, vol. 3, no. 1, pp. 2840–2843, Mar. 1993.

[4] L. L. Lewis, G. Koepf, K. B. Bhasin, and M. A. Richard, "Performance of a TlCaBaO 30 GHz 64 element antenna array," *IEEE Trans. Appl. Supercond.*, vol. 3, no. 1, Mar. 1993.

[5] R. Mailloux, *Phased Array Antenna Handbook.* Dedham, MA: Artech House, 1994.

[6] P. Bauhahn, C. Butler, V. Sokolov, and T. Contolatis, "30 GHz 5-bit monolithic phase shifters," in *IEEE MTT Monolithic Circuits Symp. Dig.*, 1985, pp. 4–7.

[7] M. J. Schindler and M. E. Miller, "A 3-bit K/Ka band MMIC phase shifter," in *IEEE 1988 Microwave and Millimeter Wave Monolithic Circuits Symp. Dig.*, 1988, pp. 95–98.

[8] J. S. Martens, V. M. Hietala, D. S. Ginley, C. P. Tigges, T. A. Plut, J. K. Truman, E. K. Track, K. H. Young, and R. T. Young, "HTS-based switched filter banks and delay lines," *IEEE Trans. Appl. Supercond.*, vol. 3, no. 1, pp. 2824–2827, Mar. 1993.

[9] J. Martens, A. Pance, G.-C. Liang, C.-F. Shih, and R. Withers, "K and V band hybrid flux flow communications subsystems," DoD SBIR Phase I Final Tech. Rep., Feb. 1994.

[10] G. F. Dionne, D. E. Oates, and D. H. Temme, "YBCO/Ferrite low-loss phase shifter," *IEEE Trans. Appl. Supercond.*, vol. 5, no. 2, pp. 2083–2086, June 1995.

[11] G. F. Dionne, D. E. Oates, D. H. Temme, and J. A. Weiss, "Ferrite-superconductor devices for advanced microwave applications," submitted to *IEEE Trans. Microwave Theory Tech.*

[12] L. Ragonese, M. Ashman, S. Wang, B. Cleaveland, D. McPherson, and P. Ho, "20 GHz HEMT low noise amplifier," Rome Laboratory Final Tech. Rep. #RL-TR-92-22, Mar. 1992.

[13] J. Krupka, R. Geyer, M. Kuhn, and J. Hinken, "Dielectric properties of single crystals of Al_2O_3, $LaAlO_3$, $NdGaO_3$, $SrTiO_3$, and MgO at cryogenic temperatures," *IEEE Trans. Microwave Theory Tech.*, vol. 42, no. 10, pp. 1886–1890, Oct. 1994.

[14] N. Newman and W. Lyons, "Review of high temperature superconducting microwave devices: Fundamental issues in materials, physics, and engineering," *J. Supercond.*, vol. 6, no. 3, 1993.

[15] J. T. Williams, "Application of high temperature superconductors in antenna systems," in *Proc. Int. Conf. Electromagnetics in Advanced Applications (ICEAA '95)*, 1995, pp. 197–204.

[16] P. S. Carter, "Mutual impedance effects in large beam scanning arrays," *IEEE Trans. Antennas Propagat.*, pp. 276–285, May 1960.

[17] D. M. Pozar and D. H. Schaubert, "Analysis of an infinite array of rectangular microstrip patches with idealized probe feeds," *IEEE Trans. Antennas Propagat.*, pp. 1101–1107, Oct. 1984.

[18] J. S. Herd and K. G. Herd, "A novel superconducting microstrip antenna geometry," in *PIERS Symp. Dig.*, Cambridge, MA, July 1991.

[19] J. S. Herd, "Full wave analysis of proximity coupled rectangular microstrip antenna arrays," *Electromagnetics*, vol. 11, no. 1, pp. 21–26, Jan. 1991.

[20] R. Jackson and D. M. Pozar, "Full wave analysis of microstrip open-end and gap discontinuities," *IEEE Trans. Microwave Theory Tech.*, vol. MTT-33, pp. 1036–1042, Oct. 1985.

[21] J. M. Pond, C. M. Krowne, and W. L. Carter, "On the application of complex resistive boundary conditions to model transmission liners consisting of very thin superconductors," *IEEE Trans. Microwave Theory Tech.*, vol. 37, no. 1, Jan. 1989.

[22] H. Y. Lee and T. Itoh, "Phenomenological loss equivalence method for planar quasitem transmission lines with a thin normal conductor or superconductor," *IEEE Trans. Microwave Theory Tech.*, vol. 37, no. 12, Dec. 1989.

[23] D. Nghiem, J. T Williams, and D. R. Jackson, "A general analysis of propagation along multiple-layer superconducting stripline and microstrip transmission lines," *IEEE Trans. Microwave Theory Tech.*, vol. 39, no. 9, Sept. 1991.

[24] L. H. Lee, S. M. Ali, and W. G. Lyons, "Full wave characterization of high T_c superconducting transmission lines," *IEEE Trans. Appl. Supercond.*, vol. 2, no. 2, July 1992.

[25] M. Davidovitz, "A low loss thermal isolator for waveguides and coaxial transmission lines," accepted for publication in *IEEE Microwave Guided Wave Lett.*

[26] E. L. Moore and D. J. Audette, "An eight channel co-boresighted mm-wave receiver system," *Microwave J.*, pp. 72–81, Oct. 1992.